Microchimica Acta (2021) 188: 171
https://doi.org/10.1007/s00604-021-04819-9

ORIGINAL PAPER

5,10,15,20-tetrakis (4-carboxyl phenyl) porphyrin–functionalized urchin-like $CuCo_2O_4$ as an excellent artificial nanozyme for determination of dopamine

Yanlei He[1] · Ning Li[1] · Xiangwei Liu[1] · Wei Chen[1] · Xixi Zhu[1] · Qingyun Liu[1]

Received: 24 January 2021 / Accepted: 2 April 2021 / Published online: 23 April 2021

Abstract

Urchin-like peroxidase mimics 5,10,15,20-tetrakis (4-carboxyl phenyl) porphyrin–functionalized $CuCo_2O_4$ nanospheres (Por-$CuCo_2O_4$) has been fabricated as an excellent visual biosensor. X-ray diffractometry (XRD), scanning electron microscopy (SEM), and X-ray photoelectron spectroscopy (XPS) have been employed to characterize the composition, morphologies, and elemental analysis of the as-synthesized Por-$CuCo_2O_4$. The catalytic activity of Por-$CuCo_2O_4$ was evaluated by the chromogenic substrate 3,3′,5,5′-tetramethylbenzidine (TMB) with the aid of H_2O_2, which exhibited a visual blue change with an absorption maximum at 652 nm for only 10 s. The peroxidase-like behaviors of Por-$CuCo_2O_4$ conformed to the Michaelis-Menten equation. Electrochemistry, radical scavenger, and fluorescence probe experiments verified that electron transfer, $\bullet O_2^-$ radicals, and holes (h^+) are the important factors during the catalytic oxidation of TMB. Based on the inhibition of dopamine (DA) on TMB oxidation, the Por-$CuCo_2O_4$-based colorimetric biosensor has been successfully constructed for sensitive determination of DA witha detection limit (LOD) of 0.94 μM. In addition, colorimetry was validated to detect DA in serum samples with high sensitivity and good selectivity.

Keywords Biosensors · Por-$CuCo_2O_4$ · Peroxidase mimic · Dopamine

Introduction

Dopamine (DA) acts as a neurotransmitter in the central nervous system, impacting physiological and neurological activities [1]. The abnormal levels of DA are able to trigger various neurological diseases, such as schizophrenia [2], cardiovascular disease [3], and Alzheimer's disease [4]. Fortunately, the relative pathological function can release a certain concentration of small biological molecules including H_2O_2, glucose, and DA. Thus, we can detect these small biological molecules as metabolic parameters for promising disease diagnosis. Accordingly, accurate quantitative determination of DA is vitally essential for clinical analysis and early diagnosis of relative diseases.

Nevertheless, the lack of electrical activity, chromophores, and fluorophores makes the detection of DA become particularly difficult. In order to efficiently detect DA, various biosensors such as electrochemistry [5], chemiluminescence, colorimetry [6], and fluorescence [7] have been developed. Among these methods, the colorimetric method has been focused on due to the unique advantages of sensitive reaction, simple preparation, intuitive, good selectivity, and low requirements on the instrument [8]. Accordingly, it is necessary to establish a novel material for DA and apply it conveniently in practice.

Nanozymes, a class of simulated enzymes with unique properties of nanomaterials, have attracted more and more attention due to their advantages in economy, stability, and catalytic activity over natural enzymes. Recently, various nanozymes including metal oxides [9], metal sulfides [10], and precious metal nanoparticles [11] have been verified to possess good peroxidase activity. Compared with single-metal nanomaterials, bimetallic nanomaterials show excellent catalytic performance. Chen et al. developed $CeCoO_3$ bimetallic nanomaterials and successfully applied them to sensitive detection of glutathione. Although many nanozymes have

✉ Qingyun Liu
qyliu@sdust.edu.cn

[1] College of Chemical and Biological Engineering, Shandong University of Science and Technology, Qingdao 266590, People's Republic of China

been explored and developed, their catalytic mechanism, sensitivity, and selectivity are still important challenges in research. Among strategies of developing the catalytic activity of nanoenzymes, organic molecules with large conjugate macrocycles have been considered attractive ones to modify some semiconductor nanomaterials [12]. Porphyrins (Por) are such ones. Porphyrins are usually used as photosensitizers to enhance the performance of some inorganic nanomaterials applied in the solar cells [13], photodynamic therapy [14], and catalysis [15], etc. Moreover, some merits including good biocompatibility and strong coordination with metals make porphyrins become ideal candidates to functionalize inorganic nanoenzymes and develop catalytic activity, accordingly [16]. Therefore, considering an interesting spinel cobaltite Por-$CuCo_2O_4$ as an excellent peroxidase, a fast colorimetric sensing platform for DA can come true.

Herein, we prepared 5,10,15,20-tetrakis (4-carboxyl phenyl) porphyrin (Fig. S1)–functionalized urchin-like $CuCo_2O_4$ nanocomposites (Scheme 1), which were verified to possess an excellent peroxidase-like activity with the aid of TMB accompanied by a color change in the process of the catalytic reaction. The catalytic performance of Por-$CuCo_2O_4$ peroxidases conforms to the Michaelis-Menten equation. Notably, the response time of blue color (oxTMB) is 10 s, a very short time, which is very important to construct a fast colorimetric sensor to realize real-time detection. Electrochemistry, radical scavenger, and fluorescence probe experiments indicate that electron transfer, $\bullet O_2^-$ radicals, and holes (h^+) are the important factors during the catalytic oxidation of TMB. In addition, based on Por-$CuCo_2O_4$ peroxidases, a fast colorimetric sensing platform for H_2O_2 and DA was developed with high sensitivity and good selectivity.

Experiment and methods

Reagents

Copper chloride dihydrate ($CuCl_2{\cdot}2H_2O$), hydrogen peroxide (H_2O_2, 30 wt.%), cobalt chloride hexahydrate ($CoCl_2{\cdot}6H_2O$), and dopamine hydrochloride were commercially provided by Aladdin Biochemical Technology Co., Ltd. 3,3′,5,5′-tetramethylbenzidine dihydrochloride (TMB•2HCl) was procured from Macklin (Shanghai, China). Ethylene diamine tetraacetic acid disodium salt (EDTA), urea, Na^+ (NaCl), K^+ (KCl), Mg^{2+} ($MgSO_4$), p-benzoquinone (PBQ), sucrose, lactose, fructose, D-histidine, L-arginine, D-serine, and isopropyl alcohol (IPA) were purchased from Sinopharm Chemical Reagent Co. Ltd. (Shanghai, China). The synthesis of 5,10,15,20-tetrakis (4-carboxyl phenyl) porphyrin (H_2TCPP) was referred to by an earlier report [17].

Characterization

The products were analyzed by a powder X-ray diffractometry (XRD) instrument (Cu-Kα, $\lambda = 1.54178$ Å) and a scanning electron microscopy instrument (APREO, American) operated at an accelerating voltage of 2 kV and is equipped with an energy-dispersive X-ray spectroscopy (EDX) instrument. The valence state of the elements in Por-$CuCo_2O_4$ was analyzed by an X-ray photoelectron spectroscopy (XPS) instrument (Thermo ESCALAB 250 Xi). The specific surface areas and pore size distribution of nanoparticles were analyzed by the Brunauer-Emmett-Teller surface areas (BET) and the Barrett-Joiner-Halenda (BJH) process with a Micromeritics ASAP 2460 analyzer. Fluorometric data (FL) and the UV-vis absorption spectrum data were obtained on a Hitachi F-4600 spectrofluorophotometer (Japan) and the TU 1810 spectrophotometer (Puxi, China), respectively. The electrochemical performance is characterized by CHI 760E Chen-Hua electrochemical workstation.

Synthesis of urchin-like Por-$CuCo_2O_4$

Firstly, urchin-like $CuCo_2O_4$ microspheres were prepared by the hydrothermal method [18]. After that, the urchin-like Por-$CuCo_2O_4$ microspheres were prepared by a two-step method. The formation process of urchin-like Por-$CuCo_2O_4$ nanospheres is shown in Scheme 1. The detailed preparation was presented in supporting information.

Scheme 1 Schematic illustration for the formation process of urchin-like Por-$CuCo_2O_4$ nanospheres

After calcination, 3 mg H_2TCPP was dissolved in NaOH alkaline water (pH = 9). After that, 60 mg of $CuCo_2O_4$ sample was added to the above solution, which was ultrasonically dissolved and transferred to a Teflon-lined autoclave with 110 °C hydrothermal for 60 min. After the sample was collected by centrifugation and further purified, Por-$CuCo_2O_4$ composite has been successfully synthesized.

Peroxidase-like activity of Por-$CuCo_2O_4$ and the DA detection

The experiment was conducted in acetic acid buffer containing Por-$CuCo_2O_4$ (0.015 mg mL^{-1}), H_2O_2 (25 mM), and TMB (0.1 mM). The visible absorption spectra were collected after the system reacted for 90 s. Kinetic experiments were carried out by measuring the absorbance at 652 nm in acetate buffer containing Por-$CuCo_2O_4$, H_2O_2, and various concentrations of TMB at room temperature. Similarly, as a control experiment, other conditions remain unchanged as described above, by changing the H_2O_2 concentration and fixing the TMB concentration. The apparent kinetic parameters were calculated by the following equation: 1 v = (K_m V_{max}) × (1 [S]) + 1 V_{max}, where v, [S], V_{max}, and K_m stand for initial velocity, the substrate concentration, the maximal velocity, and the Michaelis constant, respectively.

The DA detection is described in detail as follows: freshly prepared various concentrations of DA (10–700 μM) were added into the reaction mixture containing the buffer solution acetate (pH 4.0), Por-$CuCo_2O_4$ (0.015 mg mL^{-1}), H_2O_2 (25 mM), and TMB (0.1 mM). The entire reaction mixture was incubated for 3 min, and the absorbance of various DA concentrations was recorded.

Test of active species

A standard three-electrode system (Por-$CuCo_2O_4$-modified glassy carbon electrode, the platinum wire electrode, and the saturated calomel electrode) was used in the electrochemical experiment. In the cyclic voltammetry experiment, the current and potential responses were recorded before and after the addition of H_2O_2 to form a control group. In the amperometric testing experiment, the electrodes of uncoated and coated materials were subjected to a control test, and the electrochemical response was collected after adding the H_2O_2 (1 M) to react for 60 s. H_2O_2 (1 M) was added to PBS every 50 s, and the electrochemical response of the solution was recorded.

The capture experiments were conducted by selecting EDTA, IPA, and PBQ to capture holes (h^+), hydroxyl radicals (•OH), and superoxide radicals ($•O_2^-$), respectively. Specifically, different scavengers (200 μL) and Por-$CuCo_2O_4$ (100 μL) were injected into 2 mL of H_2O_2-TMB system to form a mixture. The absorbance at 652 nm was recorded after the above mixture reacted for 90 s at ambient temperature.

Fluorescent experiments were implemented by selecting terephthalic acid (TA) to capture •OH to form dihydroxyterephthalic acid (HOTA) with strong fluorescence. Specifically, freshly prepared various samples contain 5 mM TA, 25 mM H_2O_2, and Por-$CuCo_2O_4$ at a concentration of 0.1–0.8 mg mL^{-1} and acetate buffer at pH 4. Fluorescence spectra were recorded after the above mixtures were reacted for 30 min at the optimal temperature.

Detection of DA

The human serum samples of two volunteers were provided by the Affiliated Hospital of Qingdao University, China. To avoid the interference of coexisting substances, the resulting serum sample was diluted 80 times with PBS, which diluted DA to a certain concentration, and then added into the system containing H_2O_2-TMB. After 3 min of reaction, the absorbance of the reaction system at 652 nm was recorded.

Results and discussion

Characterization of Por-$CuCo_2O_4$ spinel microspheres

The phase of such interesting hierarchical microspheres was studied by XRD (Fig. 1a). The diffraction peaks at 19.07°, 31.36°, 36.96°, 38.96°, 45.07°, 56.03°, 59.60°, 65.70°, and 77.55° are indexed to the crystal plane of (111), (220), (311), (222), (400), (422), (511), (440), and (533) of cubic $CuCo_2O_4$ phase (JCPDS card no. 01-1155) [19]. Carefully, one diffraction peak at 35.55° is attributed to monoclinic CuO (JPCDS card no. 05-0661) [20]. Therefore, the main composition of nanocomposites is $CuCo_2O_4$, accompanied by trace amounts of CuO [21], because $CuCo_2O_4$ has poor thermal stability and is easy to produce CuO [22]. Notably, the XRD peaks of Por-$CuCo_2O_4$ are almost consistent with that of $CuCo_2O_4$, suggesting that the introduction of porphyrin has no effect on the lattice structure of the composites, due to a small quantity of porphyrin in the composites.

XPS is used to further study the composition and oxidation states of Por-$CuCo_2O_4$, shown in Fig. 1b–f. The survey spectra in Fig. 1b display the composition of Cu, Co, O, and N elements in $CuCo_2O_4$ and Por-$CuCo_2O_4$, respectively. In the Cu 2p spectra (Fig. 1c), two major spin-orbit doublets with binding energy at approximately 935.1 and 933.7 eV are ascribed to Cu^{2+} and Cu^+ [23]. The Gaussian fitting curves show that the Co 2p spectra (Fig. 1d) are composed of Co $2p_{3/2}$ and Co $2p_{1/2}$ peaks at 935.1 and 933.7 eV with two satellite peaks located at approximately 941.2 and 943.8 eV [24]. As seen from Fig. 1e, the O1s spectrum can be fitted to three Gauss peaks at 532.7 eV, 531.3 eV, and 529.8 eV, which are

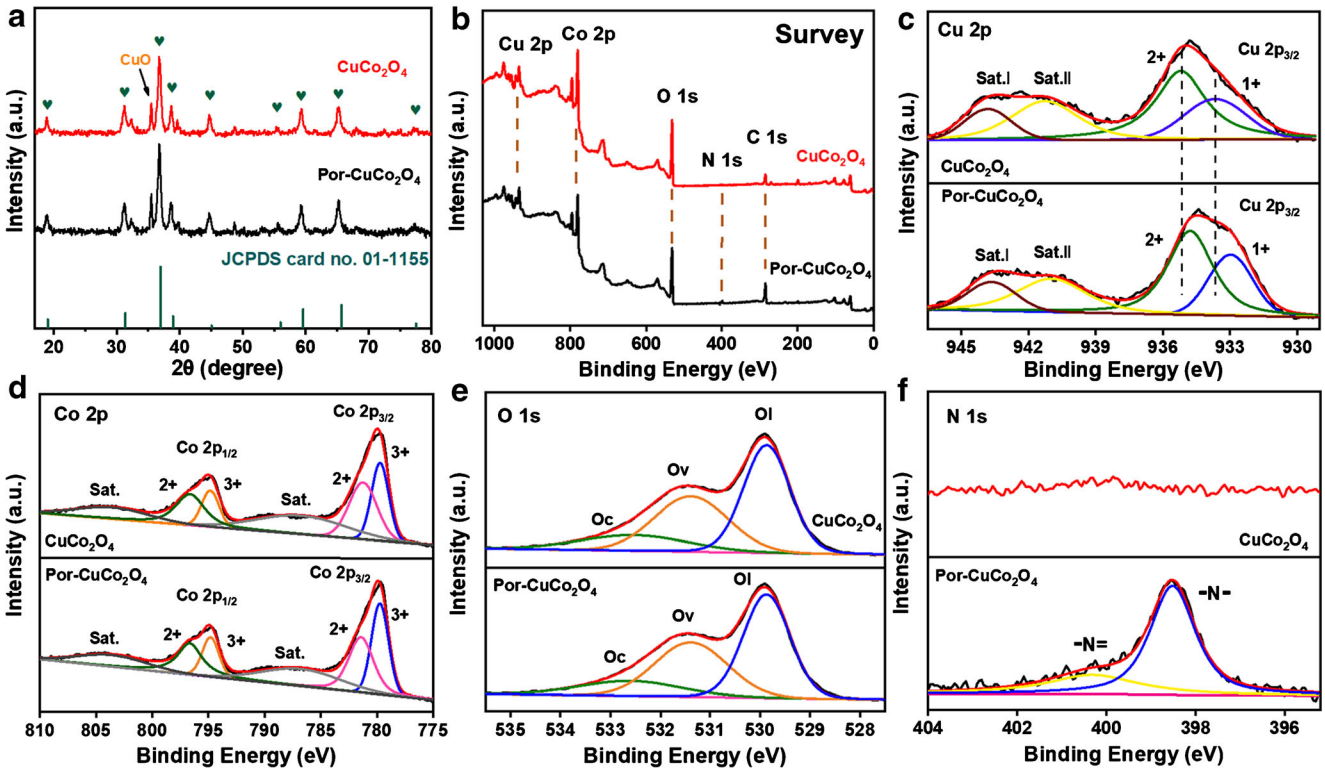

Fig. 1 XRD (**a**) and XPS spectra data of the as-prepared $CuCo_2O_4$ and Por-$CuCo_2O_4$ nanocomposites: Survey scan spectra (**b**), Cu 2p (**c**), Co 2p (**d**), O 1s (**e**), and N 1s (**f**), respectively

attributed to chemisorbed oxygen, the oxygen vacancy, and the lattice oxygen [25], respectively. The existence of oxygen vacancy is in favor of the improvement of the catalytic activity of Por-$CuCo_2O_4$. Figure 1f shows the comparison spectra of N 1s in $CuCo_2O_4$ and Por-$CuCo_2O_4$. Compared with that of $CuCo_2O_4$, N 1s in Por-$CuCo_2O_4$ has peaks at bond energy of 398.5 eV and 400.4 eV, corresponding to the -N- bond and the -N = bond of the porphyrin ring [17], indicating that the porphyrin was successfully introduced.

Morphologies of $CuCo_2O_4$ and Por-$CuCo_2O_4$ were analyzed by SEM and TEM, respectively. As displayed in Fig. 2a and b, $CuCo_2O_4$ and Por-$CuCo_2O_4$ all exhibit urchin-like microsphere structure with 5–10 μm in size, which are composed of needle-like nanorods. Carefully, TEM images (Fig. 2c and d) display that needle-like nanorods are further composed of a lot of nanoparticles. From the HRTEM image of Por-$CuCo_2O_4$ (Fig. 2e), the lattice fringes of 0.456 nm, 0.284 nm, and 0.243 nm are in accordance with the crystalline planes of (111), (220), and (311) of $CuCo_2O_4$ in XRD data, respectively. Subsequently, the EDX element mapping (Fig. 2f) shows that Cu, Co, O, and N elements uniformly distribute Por-$CuCo_2O_4$ composite, indicating the successful preparation of Por-$CuCo_2O_4$. Additionally, the calculated BET specific surface area (Fig. S2a) of Por-$CuCo_2O_4$ composite material is 45.57 $m^2\ g^{-1}$, which is much larger than pure $CuCo_2O_4$ (36.56 $m^2\ g^{-1}$). In addition, the Barrett-Joiner-Halenda (BJH) model calculates that the Por-$CuCo_2O_4$ pore size distribution is about 2 nm and 6.9 nm in diameter (Fig. S2b). It can be seen that the introduction of porphyrin further increases the specific surface area of Por-$CuCo_2O_4$ and provides more active sites.

Peroxidase-like activity

In order to validate the peroxidase-like activity of Por-$CuCo_2O_4$, six reaction systems were devised as control experiments using TMB as the chromogenic substrate, which can be oxidized to generate blue oxTMB with a distinct absorption at 652 nm. As seen from curves 3c–3f in Fig. 3, four systems hardly have absorption in the absence of H_2O_2 or composites ($CuCo_2O_4$, Por-$CuCo_2O_4$), suggesting that either individual H_2O_2 or nanocomposite cannot trigger the oxidation reaction of TMB. Interestingly, systems a and b (curves 4a and 4b) have stronger absorption intensity accompanied by a marked color change (illustration), indicating that both $CuCo_2O_4$ and Por-$CuCo_2O_4$ possess the peroxidase-like activity. Moreover, the absorption intensity of Por-$CuCo_2O_4$ (system a) is more than twice that of $CuCo_2O_4$ (system b), which indicates that Por-$CuCo_2O_4$ has a stronger peroxidase-like activity. Therefore, the simultaneous existence of Por-$CuCo_2O_4$ peroxidases and H_2O_2 is the basic condition for the rapid oxidation of TMB. The reason why Por-$CuCo_2O_4$ has more excellent peroxidase-like activity is ascribed to a lot of oxygen vacancies verified by XPS as well as the synergetic effect between

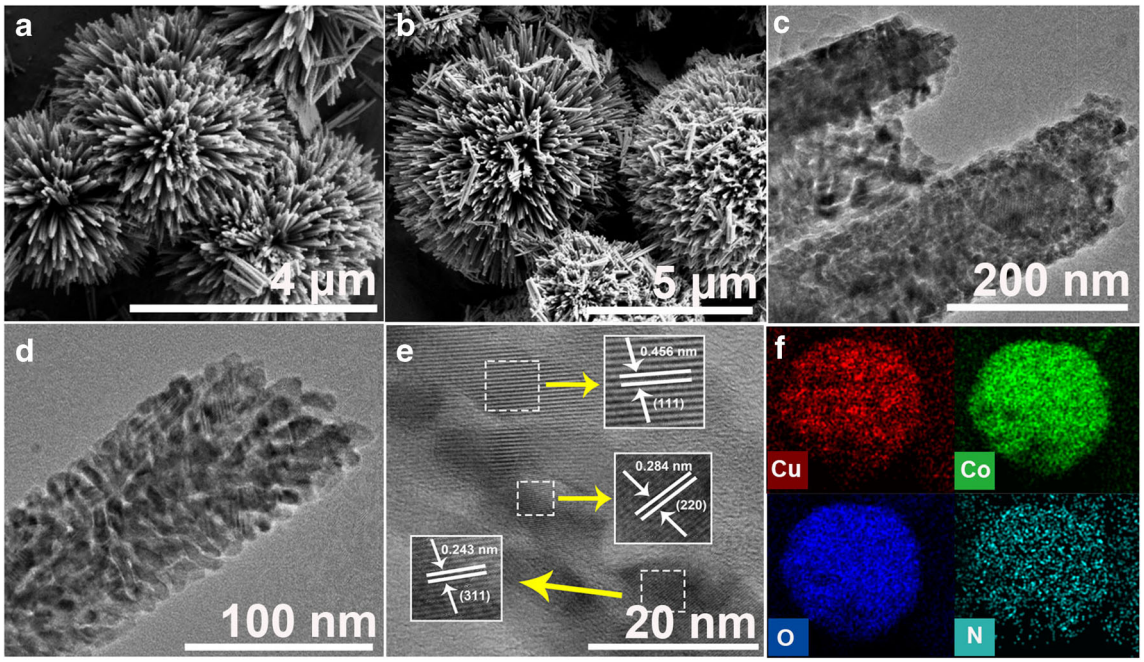

Fig. 2 SEM images of $CuCo_2O_4$ (**a**) and Por-$CuCo_2O_4$ (**b**), respectively. TEM images of $CuCo_2O_4$ (**c**) and Por-$CuCo_2O_4$ (**d**, **e**). EDX mapping images (**f**) of elements of Por-$CuCo_2O_4$: Cu, Co, O, and N

$CuCo_2O_4$ and H_2TCPP molecules, which is further explained in the catalytic section, subsequently. The according color of different reaction systems can be quickly distinguished in 90 s, shown in the inset of Fig. 3. As we know, the catalytic activity of artificial peroxidase and natural peroxidase is influenced by pH and temperature. Figure S3 shows that pH = 4 and 45 °C are the best conditions, which will be applied to subsequent experiments.

The steady-state kinetics of Por-$CuCo_2O_4$ was studied by keeping the TMB concentration constant while changing the H_2O_2 concentration (and vice versa). Figure 4a and c respectively show the relationship between the concentration of

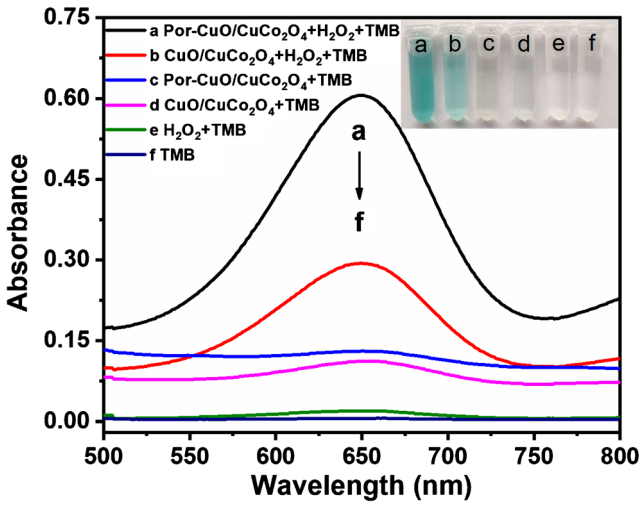

Fig. 3 UV-visible absorption spectra and corresponding photograph of color change of different reaction systems in 90 s

H_2O_2 and TMB as substrates and the initial reaction rate. The values of K_m and V_{max} were calculated according to the Michaelis-Menten equation (Fig. 4b and d). In comparison with the affinity of HRP together with other artificial peroxidase, some related parameters are shown in Table S1. Compared with that of HRP and other artificial peroxidase ($Cu(OH)_2$, Co_3O_4@CeO_2, PtCNPs, [Cu(PDA)(DMF)]), our obtained Por-$CuCo_2O_4$ has the lower K_m value, indicating that Por-$CuCo_2O_4$ has a stronger affinity towards TMB, which is a favorable factor for catalytic enhancement of Por-$CuCo_2O_4$.

Colorimetric detection of small biological molecules and selective exploration

As an oxidant, H_2O_2 is not only used in industrial production but also plays a key role in biological processes. However, long-term excessive use of H_2O_2 can cause diseases such as low immunity, genetic mutations, arteriosclerosis, and diabetes [26]. Therefore, designing a fast colorimetric sensing platform for H_2O_2 is particularly important. Herein, based on Por-$CuCo_2O_4$ with higher peroxidase-like activity, a series of experiments (Fig. 5a) were designed and implemented by changing the concentration of H_2O_2 (0.1–10 mM). From the data, a very good linear relationship (inset) of absorbance and H_2O_2 concentration in the concentration range of 0.1–1.0 mM (R^2 = 0.998) was obtained. The detection limit (LOD) is calculated to be 90.26 μM (LOD = 3 s/k), suggesting a good sensitivity of the constructed colorimetric sensor based on Por-$CuCo_2O_4$ to the TMB-H_2O_2 system.

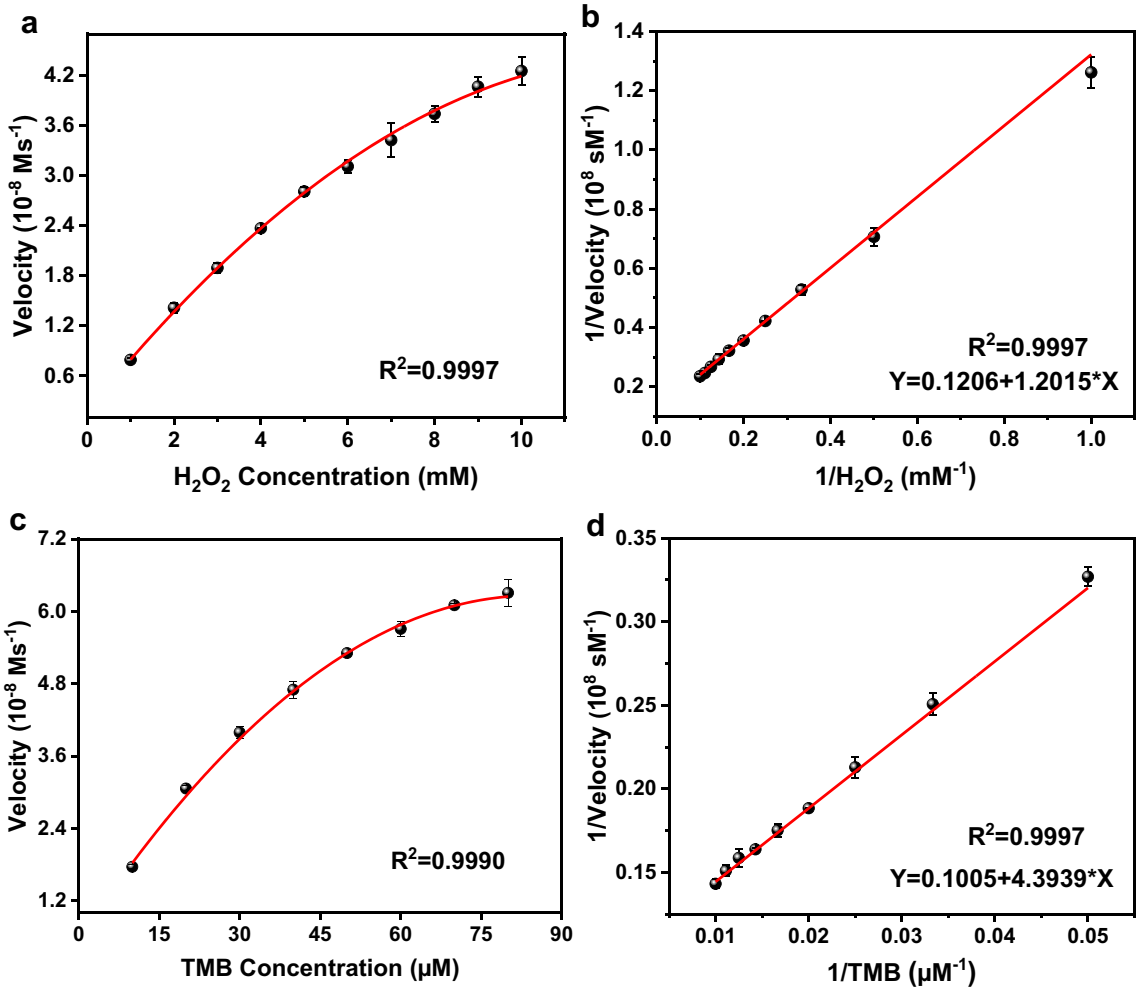

Fig. 4 Steady-state kinetic tests of Por-$CuCo_2O_4$ using Michaelis-Menten model. **a** The concentration of TMB was 100 μM and varying the H_2O_2 concentration from 1 to 10 mM. **b** The corresponding double reciprocal curves for H_2O_2. **c** The concentration of H_2O_2 was 35 mM and varying the TMB concentration from 10 to 100 μM. **d** The corresponding double reciprocal curves for TMB. Error bars represent the standard deviation for three measurements. The data was collected at 652 nm

As a neurotransmitter, DA as a necessary substance for our body can regulate various physiological functions of the central nervous system. Therefore, a simple method for rapid determination of DA is meaningful. Therefore, a series of experiments were carried out by tuning DA concentration (10–700 μM) under the optimal conditions (pH = 4 and 45 °C). Because phenol hydroxyl and amino groups are attached in the molecule structure of DA, DA molecules exhibit reducibility. Thus, in our designed sensing system (DA + Por-$CuCo_2O_4$ + H_2O_2 + TMB), DA molecules can prevent TMB from being oxidized by H_2O_2, resulting in a reduction of the oxTMB absorbance together with fading of blue color visually [27]. The response curve of DA concentration and absorbance difference value ΔA ($\Delta A = A_{blank} - A_{DA}$) has a good linear relationship at 10–100 μM (inset of Fig. 5b). In addition, compared with that of DA measured by different methods (colorimetry, fluorimetry, and electrochemistry) in different catalyst systems (Co_3O_4@NiO, CeO_2, Pt/$CoSn(OH)_6$, ZnO@Cys NPs, Pdots@AMP-Cu, RGO-ZnO, CRGO-Au NCs, Ag/rGO) listed in Table S2, a lower LOD (0.94 μM, S/N = 3) of the Por-$CuCo_2O_4$-based colorimetric sensor was found. As we know, electrochemistry method is known as high sensitivity. Expectably, our designed colorimetric sensing platform for DA was on a par with the electrochemistry method.

Other than high sensitivity, good selectivity is also necessary for colorimetric sensors. From Fig. 5c and d, absorbance difference value ΔA of two systems is the highest and hardly influenced in the presence of common interfering molecules (Suc, Fru, Lac Arg, Ser, His, Na^+, K^+, Mg^{2+}, UA, ISO, Leu), even though their concentration is 10 times than that of H_2O_2 and DA, respectively. Nevertheless, this method is still a big challenge for distinguishing DA and materials with reducing substances. It is suggested that the colorimetric sensing platform has good selectivity for the determination of H_2O_2 and DA in the absence of reducing substances.

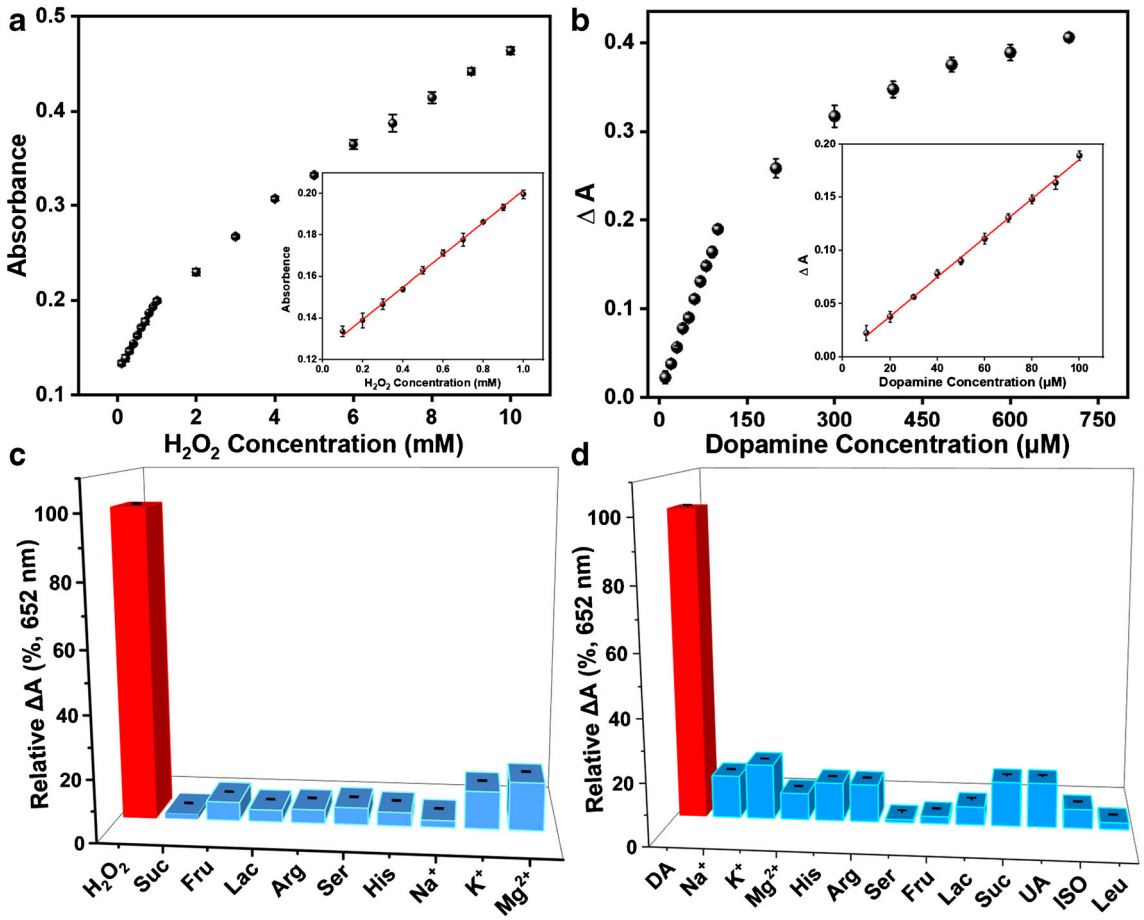

Fig. 5 Dose-response curve for H_2O_2 (**a**) and or DA (**b**) determination at 652 nm. **b** ΔA response of H_2O_2-TMB system towards different DA concentrations from 10 to 700 μM; the inset is the linear fitting curve from 10 to 100 μM. The variance of net absorbance (ΔA) in the presence of various substances. $\Delta A = A_0 - A$, where A_0 and A are the absorbance of the Por-$CuCo_2O_4$ system at 652 nm in the presence and absence of DA. **c** The selectivity of the Por-$CuCo_2O_4$ towards H_2O_2 (0.1 mM) and interferents (1.0 mM). **d** The selectivity of the Por-$CuCo_2O_4$ towards DA (1.0 mM) and interferents (10 mM). Error bars denote standard deviations based on three measurements

Proposed mechanism

According to publications, the catalytic mechanism of artificial peroxidases is ascribed to two kinds as follows: one is from direct electron transfer between the substrates and reactants. The other is due to some active species during the catalytic reaction. Therefore, the possible catalytic mechanisms need to be verified one by one. Firstly, an electron transfer process was studied by electrochemical methods (cyclic voltammetry and amperometric methods). In the cyclic voltammetry experiment (Fig. 6a), the Por-$CuCo_2O_4$ modified electrode (control group) has no obvious current in the absence of H_2O_2. Nevertheless, after adding 1 M H_2O_2, a clear current response with an obvious redox peak at −0.45 eV was obtained, indicating that Por-$CuCo_2O_4$ has the ability to transfer electrons between the electrode surface (electron donor) and H_2O_2 (electron acceptor) [28]. At −0.45 eV, the ampere experiment of Por-$CuCo_2O_4$ catalyzed bare GCE and Por-$CuCo_2O_4$ modified GCE (Por-$CuCo_2O_4$/GCE) is shown in Fig. 6b. Adding H_2O_2 every 50 s, the reduction current in the Por-$CuCo_2O_4$/GCE electrode increases steadily with a high sensitivity. The data suggest that Por-$CuCo_2O_4$ peroxidases can speed up electron transfer.

Secondly, to study the possible active species produced in the process of Por-$CuCo_2O_4$ catalytic reaction, various capture experiments were implemented. Based on the previous results and our constructed colorimetric sensing system, three active species, namely, holes (h^+), superoxide radicals ($\bullet O_2^-$), and hydroxyl radicals (•OH), are produced, and the catalytic system may exist during the catalytic reaction. The active species including h^+, $\bullet O_2^-$, and •OH can be captured by trapping agents PBQ, EDTA, and IPA, respectively. If three active species are produced during the catalytic reaction, the absorbance of the catalytic system will be decreased by addition of the trapping agents. Obviously, as seen from Fig. 6c, $\bullet O_2^-$ and h^+ play an important role while •OH is not detected by the trapping agent method. In order to further determine whether the catalytic oxidation of TMB by Por-$CuCo_2O_4$ nanospheres is based on the hydroxyl (•OH) mechanism, terephthalic acid (TA) was selected as the trapping agent. It is known that the

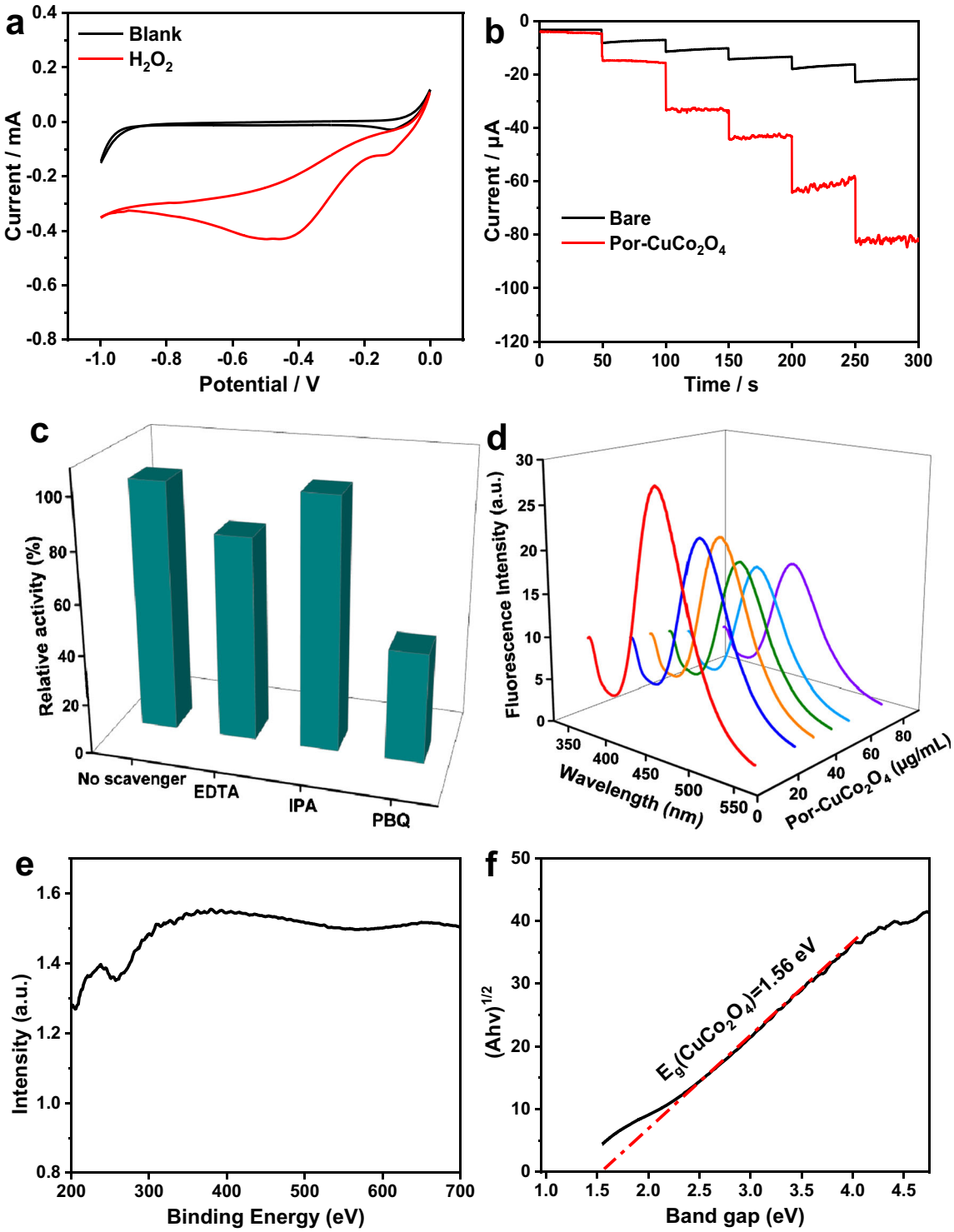

Fig. 6 **a** Cyclic voltammetry of Por-$CuCo_2O_4$/GCE in 40 mL PBS in the absence (blank) and in the presence (red) of 1 M H_2O_2 (scan rate: 0.05 V/s). **b** The typical steady-state current response of the Por-$CuCo_2O_4$/GCE to the successive addition of H_2O_2 (1 M) every 50 s into the PBS under stirring at the applied potential of −0.45 V. **c** Effects of various active scavengers during the catalysis of TMB with the aid of Por-$CuCo_2O_4$. **d** Fluorescence intensity varies with the concentration of Por-$CuCo_2O_4$ at different wavelengths. **e** The UV-vis DRS spectra and **f** Tauc plots of $CuCo_2O_4$

resulting •OH reacts with TA, a non-fluorescent molecule, to form highly fluorescent hydroxy terephthalate acid (HTA), which shows an emission maximum at 432 nm when excited at 315 nm [29]. Figure 6d shows the relationship of the fluorescence intensity and Por-$CuCo_2O_4$ concentration. As seen from the figure, the fluorescence intensity is decreased with

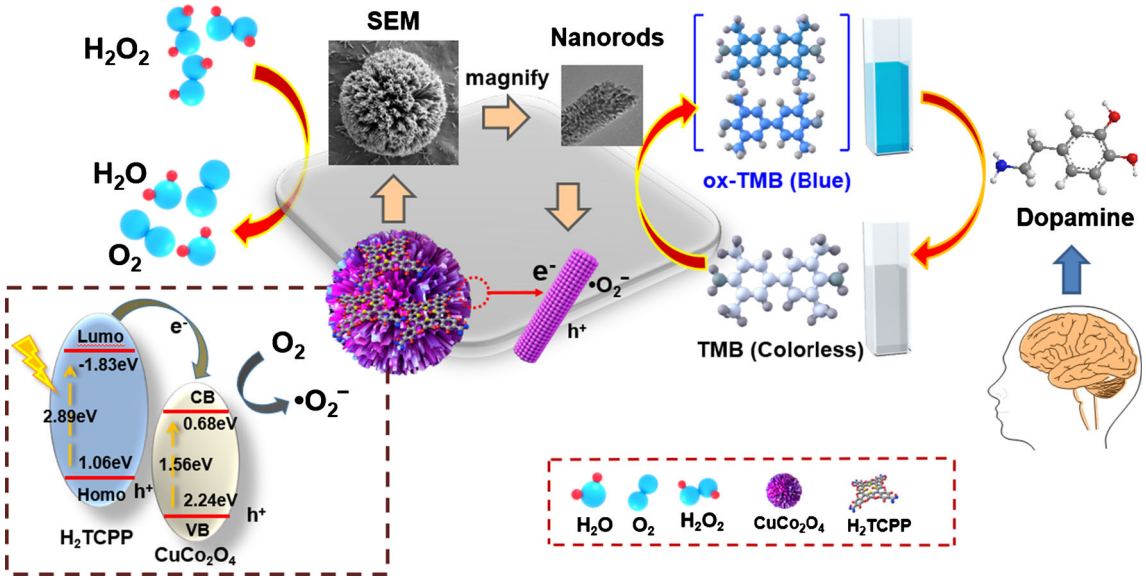

Scheme 2 Schematic illustration of Por-$CuCo_2O_4$ as a peroxidase mimic for H_2O_2 and dopamine detection

increasing of Por-$CuCo_2O_4$ concentration (10–80 μg/mL), further suggesting that •OH does not exist during the catalytic reaction. The fluorescence result is consistent with the capture experiment. Therefore, based on the results, the catalytic mechanism of Por-$CuCo_2O_4$ is not only from the direct electron transfer between reactants but also from two active species ($\bullet O_2^-$ and h^+) produced in the course of the catalytic reaction.

According to the UV-vis diffuse reflectance spectra and Tauc plots (Fig. 6e and f), the forbidden bandwidth (E_g) of the $CuCo_2O_4$ is determined to be 1.56 eV [30]. Through the following Mulliken electronegativity theory formula (E_0 = 4.5 eV, X is the geometric mean of the absolute electronegativity of the constituent atoms in $CuCo_2O_4$), the valence band position (VB) and conduction band (CB) position of $CuCo_2O_4$ are located at 2.24 and 0.68 eV, respectively [31]. The position of the conduction band valence band of H_2TCPP refers to previous publications [32].

$$E_{VB} = X - E_0 + 0.5E_g$$
$$E_{CB} = E_{VB} - E_g$$

Based on the mentioned information, a catalytic mechanism of Por-$CuCo_2O_4$ is proposed (Scheme 2). As we know, porphyrin molecules have absorption in the visible region and are usually considered photosensitizers. Thus, the electrons on HOMO can jump into LUMO of the porphyrin under visible light, resulting in the production of h^+. At the same time, the unstable electrons on LUMO of porphyrin are further rapidly transferred to the CB of $CuCo_2O_4$. TMB adsorbed on the surface of Por-$CuCo_2O_4$ due to the accumulation effect provides the lone electron pair in the amino group to Por-$CuCo_2O_4$, increasing its electron density and mobility [33]. After that, the electron-rich Por-$CuCo_2O_4$ center can make electrons be transferred to H_2O_2, thereby reducing it to oxygen [34]. Furthermore, the transferred electrons reduced O_2 into $\bullet O_2^-$ radicals, due to the a lot of oxygen vacancies that existed in Por-$CuCo_2O_4$. In addition, due to the quantum size effect, the large specific surface area, and small crystal size, Por-$CuCo_2O_4$ composed of a lot of smaller nanoparticles can provide much more catalytic active sites, thereby binding substrates with smaller steric hindrance and stronger redox

Table 1 Results of dopamine detection in human serum samples

Sample	Detected (μM)	Spiked (μM)	Found (μM)	Recovery (%)	RSD (%) (n=3)
Sample 1	ND	35	33.82±0.36	96.64	0.91
	ND	55	51.94±0.54	94.44	1.03
	ND	75	67.70±1.09	90.27	1.59
Sample 2	ND	20	21.87±0.91	109.34	3.67
	ND	40	35.45±0.90	88.64	2.29
	ND	60	56.29±2.17	93.81	3.43

Note: Serums are obtained from the Affiliated Hospital of Medical College Qingdao University, China

capacity [33]. In addition, based on the reducing property of DA (which can fade blue oxTMB), sensitive and selective detection of DA can come true.

Determination of DA in serum

Before determination, the DA is dissolved into the serum to make a standard solution and then diluted to different concentrations within the linear range. The accuracy of this method can be measured by the recovery and relative standard deviation (RSD) between the determined concentration and the standard concentration [35]. As displayed in Table 1, the recovery rate and RSD are in the range of 88.64–109.34% and 0.91–3.67%, respectively. Therefore, the recoveries are acceptable, and the Por-$CuCo_2O_4$-based colorimetric sensing platform can be used to determine DA in real samples, which has a good application prospect in biological monitoring.

Conclusions

A novel urchin-like Por-$CuCo_2O_4$ with enhanced peroxidase-like activity was successfully synthesized by a simple hydrothermal method. Due to the synergistic effect between H_2TCPP molecules and $CuCo_2O_4$ under visible light, a large amount of active free radical species ($\bullet O_2^-$ and h^+) was produced and improved to the catalytic activity of Por-$CuCo_2O_4$. Even in a wide temperature range (35–55 °C), the relative activity of Por-$CuCo_2O_4$ is still higher than 90%. The TMB + Por-$CuCo_2O_4$ colorimetric sensing platform has high selectivity and good sensitivity and can accurately determine H_2O_2 and DA, and its detection limits are 90.26 μM and 0.94 μM, respectively. In addition, the determination of DA in serum has achieved satisfactory results. We believe that this work will help the design of other artificial mimic with enzyme activity and be used for real-time monitoring of certain key biomolecules related to H_2O_2 in the fields of medicine and food.

Supplementary Information The online version contains supplementary material available at https://doi.org/10.1007/s00604-021-04819-9.

Funding This work was financially supported by SNFC (21971152, 21805168, and 51904175) and the Natural Science Foundation of Shandong Province (ZR2018MB002, ZR2018MEE003, ZR2018BB046, and ZR2018PEE006).

Compliance with ethical standards

Conflict of interest The authors declare no competing interests.

References

1. Rostami S, Mehdinia A, Niroumand R, Jabbari A (2020) Enhanced LSPR performance of graphene nanoribbons-silver nanoparticles hybrid as a colorimetric sensor for sequential detection of dopamine and glutathione. Anal Chim Acta 1120:11–23. https://doi.org/10.1016/j.aca.2020.04.060
2. Wang Y, Yang L, Liu Y, Zhao Q, Ding F, Zou P, Rao H, Wang X (2018) Colorimetric determination of dopamine by exploiting the enhanced oxidase mimicking activity of hierarchical $NiCo_2S_4$-rGO composites. Mikrochim Acta 185(10):496. https://doi.org/10.1007/s00604-018-3035-8
3. Liu H, Ding YN, Bian B, Li L, Li R, Zhang X, Liu Z, Zhang X, Fan G, Liu Q (2019) Rapid colorimetric determination of dopamine based on the inhibition of the peroxidase mimicking activity of platinum loaded $CoSn(OH)_6$ nanocubes. Mikrochim Acta 186(12):755. https://doi.org/10.1007/s00604-019-3940-5
4. Belujon P, Grace AA (2017) Dopamine system dysregulation in major depressive disorders. Int J Neuropsychopharmacol 20(12):1036–1046. https://doi.org/10.1093/ijnp/pyx056
5. Qing X, Wang Y, Zhang Y, Ding X, Zhong W, Wang D, Wang W, Liu Q, Liu K, Li M, Lu Z (2019) Wearable fiber-based organic electrochemical transistors as a platform for highly sensitive dopamine monitoring. ACS Appl Mater Interfaces 11(14):13105–13113. https://doi.org/10.1021/acsami.9b00115
6. Wen D, Liu W, Herrmann AK, Haubold D, Holzschuh M, Simon F, Eychmuller A (2016) Simple and sensitive colorimetric detection of dopamine based on assembly of cyclodextrin-modified au nanoparticles. Small 12(18):2439–2442. https://doi.org/10.1002/smll.201503874
7. Zhao J, Zhao L, Lan C, Zhao S (2016) Graphene quantum dots as effective probes for label-free fluorescence detection of dopamine. Sensors Actuators B Chem 223:246–251. https://doi.org/10.1016/j.snb.2015.09.105
8. Ding Y, Yang B, Liu H, Liu Z, Zhang X, Zheng X, Liu Q (2018) FePt-Au ternary metallic nanoparticles with the enhanced peroxidase-like activity for ultrafast colorimetric detection of H_2O_2. Sensors Actuators B Chem 259:775–783. https://doi.org/10.1016/j.snb.2017.12.115
9. Zhang L, Zhong H, Zhang H, Ding C (2021) A multifunctional nano system based on DNA and CeO_2 for intracellular imaging of miRNA and enhancing photodynamic therapy. Talanta 221:121554. https://doi.org/10.1016/j.talanta.2020.121554
10. Jiao Y, Li J, Xiang J, Chen Z (2020) Tungsten disulfide nanosheets-based colorimetric assay for glucose sensing. Spectrochim Acta A Mol Biomol Spectrosc 242:118706. https://doi.org/10.1016/j.saa.2020.118706
11. Zeng G, Duan M, Xu Y, Ge F, Wang W (2020) Platinum (II)-doped graphitic carbon nitride with enhanced peroxidase-like activity for detection of glucose and H_2O_2. Spectrochim Acta A Mol Biomol Spectrosc 241:118649. https://doi.org/10.1016/j.saa.2020.118649
12. Guo Y, Deng L, Li J, Guo S, Wang E, Dong S (2011) Hemin?graphene hybrid nanosheets with intrinsic peroxidase-like activity for label-free colorimetric detection of single-nucleotide polymorphism. ACS Nano 5(2):1282–1290
13. Yella A, Lee HW, Tsao HN, Yi C, Chandiran AK, Nazeeruddin MK, Diau EWG, Yeh CY, Zakeeruddin SM, Gratzel M (2011) Porphyrin-sensitized solar cells with cobalt (II/III)-based redox electrolyte exceed 12 percent efficiency. Science 334(6056):629–634. https://doi.org/10.1126/science.1209688
14. Alemayehu AB, Day NU, Mani T, Rudine AB, Thomas KE, Gederaas OA, Vinogradov SA, Wamser CC, Ghosh A (2016) Gold Tris (carboxyphenyl) corroles as multifunctional materials: room temperature near-IR phosphorescence and applications to photodynamic therapy and dye-sensitized solar cells. ACS Appl

Mater Interfaces 8(29):18935–18942. https://doi.org/10.1021/acsami.6b04269
15. Azcarate I, Costentin C, Robert M, Saveant JM (2016) Through-space charge interaction substituent effects in molecular catalysis leading to the design of the most efficient catalyst of CO_2-to-CO electrochemical conversion. J Am Chem Soc 138(51):16639–16644. https://doi.org/10.1021/jacs.6b07014
16. Zhu X, Li H, Zhang D, Chen W, Fu M, Nie S, Gao Y, Liu Q (2019) Novel "on–off" colorimetric sensor for glutathione based on peroxidase activity of Montmorillonite-loaded TiO_2 functionalized by porphyrin precisely controlled by visible light. ACS Sustain Chem Eng 7(21):18105–18113. https://doi.org/10.1021/acssuschemeng.9b05146
17. He Y, Li N, Li W, Zhang X, Zhang X, Liu Z, Liu Q (2021) 5,10,15,20-tetrakis (4-carboxylphenyl) porphyrin functionalized $NiCo_2S_4$ yolk-shell nanospheres: excellent peroxidase-like activity, catalytic mechanism and fast cascade colorimetric biosensor for cholesterol. Sensors Actuators B Chem 326. https://doi.org/10.1016/j.snb.2020.128850
18. Song Y, Zhao M, Li H, Wang X, Cheng Y, Ding L, Fan S, Chen S (2018) Facile preparation of urchin-like $NiCo_2O_4$ microspheres as oxidase mimetic for colormetric assay of hydroquinone. Sensors Actuators B Chem 255:1927–1936. https://doi.org/10.1016/j.snb.2017.08.204
19. Chen C, Liu L, Li Y, Li W, Zhou L, Lan Y, Li Y (2020) Insight into heterogeneous catalytic degradation of sulfamethazine by peroxymonosulfate activated with $CuCo_2O_4$ derived from bimetallic oxalate. Chem Eng J 384. https://doi.org/10.1016/j.cej.2019.123257
20. Qi Y, Mei Y, Li J, Yao T, Yang Y, Jia W, Tong X, Wu J, Xin B (2019) Highly efficient microwave-assisted Fenton degradation of metacycline using pine-needle-like $CuCo_2O_4$ nanocatalyst. Chem Eng J 373:1158–1167. https://doi.org/10.1016/j.cej.2019.05.097
21. Goudarzi M, Salavati-Niasari M, Yazdian F, Amiri M (2019) Sonochemical assisted thermal decomposition method for green synthesis of $CuCo_2O_4$/CuO ceramic nanocomposite using Dactylopius Coccus for anti-tumor investigations. J Alloys Compd 788:944–953. https://doi.org/10.1016/j.jallcom.2019.02.288
22. Nakhowong R, Chueachot R (2017) Synthesis and magnetic properties of copper cobaltite ($CuCo_2O_4$) fibers by electrospinning. J Alloys Compd 715:390–396. https://doi.org/10.1016/j.jallcom.2017.04.323
23. Zhen S-y, Wu H-t, Wang Y, Li N, Chen H-s, Song W-l, Wang Z-h, Sun W, Sun K-n (2019) Metal–organic framework derived hollow porous CuO–$CuCo_2O_4$ dodecahedrons as a cathode catalyst for Li–O_2 batteries. RSC Adv 9(29):16288–16295. https://doi.org/10.1039/c9ra02860a
24. Han X, Sheng H, Yu C, Walker TW, Huber GW, Qiu J, Jin S (2020) Electrocatalytic oxidation of glycerol to formic acid by $CuCo_2O_4$ spinel oxide nanostructure catalysts. ACS Catal 10(12):6741–6752. https://doi.org/10.1021/acscatal.0c01498
25. Alali KT, Lu Z, Zhang H, Liu J, Liu Q, Li R, Aljebawi K, Wang J (2017) P–p heterojunction CuO/$CuCo_2O_4$ nanotubes synthesized via electrospinning technology for detecting n-propanol gas at room temperature. Inorg Chem Front 4(7):1219–1230. https://doi.org/10.1039/c7qi00192d
26. Ma D, Yu J, Yin W, Zhang X, Mei L, Zu Y, An L, Gu Z (2018) Synthesis of surface-modification-oriented nanosized molybdenum disulfide with high peroxidase-like catalytic activity for H_2O_2 and cholesterol detection. Chemistry 24(59):15868–15878. https://doi.org/10.1002/chem.201803040
27. Zhu Y, Yang Z, Chi M, Li M, Wang C, Lu X (2018) Synthesis of hierarchical Co_3O_4@NiO core-shell nanotubes with a synergistic catalytic activity for peroxidase mimicking and colorimetric detection of dopamine. Talanta 181:431–439. https://doi.org/10.1016/j.talanta.2018.01.019
28. Mu J, Wang Y, Zhao M, Zhang L (2012) Intrinsic peroxidase-like activity and catalase-like activity of Co_3O_4 nanoparticles. Chem Commun (Camb) 48(19):2540–2542. https://doi.org/10.1039/c2cc17013b
29. Hu AL, Liu YH, Deng HH, Hong GL, Liu AL, Lin XH, Xia XH, Chen W (2014) Fluorescent hydrogen peroxide sensor based on cupric oxide nanoparticles and its application for glucose and L-lactate detection. Biosens Bioelectron 61:374–378. https://doi.org/10.1016/j.bios.2014.05.048
30. Xue W, Chang W, Hu X, Fan J, Bai X, Liu E (2020) Highly dispersed copper cobalt oxide nanoclusters decorated carbon nitride with efficient heterogeneous interfaces for enhanced H_2 evolution. J Colloid Interface Sci 576:203–216. https://doi.org/10.1016/j.jcis.2020.04.111
31. Xu C, Jin C, Chang W, Hu X, Deng H, Liu E, Fan J (2019) Interfacially bonded $CuCo_2O_4$/TiO_2 nanosheet heterostructures for boosting photocatalytic H_2 production. Catal Sci Technol 9(18):4990–5000. https://doi.org/10.1039/c9cy01209e
32. Yang H, Yin D, Gao L, Zhang X, Zhang X, Liu Q (2020) 5,10,15,20-tetrakis(4-carboxylphenyl) porphyrin modified nickel-cobalt layer double hydroxide nanosheets as enhanced photoelectrocatalysts for methanol oxidation under visible-light. J Colloid Interface Sci 561:881–889. https://doi.org/10.1016/j.jcis.2019.11.071
33. Aneesh K, Rao vusa CS, Berchmans S (2017) Enhanced peroxidase-like activity of $CuWO_4$ nanoparticles for the detection of NADH and hydrogen peroxide. Sensors Actuators B Chem 253:723–730. https://doi.org/10.1016/j.snb.2017.06.175
34. Song Y, Qu K, Zhao C, Ren J, Qu X (2010) Graphene oxide: intrinsic peroxidase catalytic activity and its application to glucose detection. Adv Mater 22(19):2206–2210. https://doi.org/10.1002/adma.200903783
35. Rostami S, Mehdinia A, Jabbari A (2020) Intrinsic peroxidase-like activity of graphene nanoribbons for label-free colorimetric detection of dopamine. Mater Sci Eng C Mater Biol Appl 114:111034. https://doi.org/10.1016/j.msec.2020.111034